Original Article

Institution of MECHANICAL ENGINEERS
Journal of ENGINEERING TRIBOLOGY

Proc IMechE Part J:
J Engineering Tribology
1–10

DOI: 10.1177/13506501251364990
journals.sagepub.com/home/pij
Sage

Tribological performance of macro-grooved surfaces under lubricated line contact: An experimental and numerical study

Xiang Li[1,2], Zeeshan Anjum[2], Qingwen Dai[1,2], Wei Huang[1,2] and Xiaolei Wang[1,2]

Abstract

In this study, the tribological behavior of macro-grooved textures were studied using a cylinder-on-plate contact configuration (line contact) under lubrication condition. The effects of actual contact line length and groove distribution on the coefficient of friction (CoF) were investigated. The experimental results exhibited a reduction in the CoF for all of the textured samples. An increase in the number of grooves resulted into a reduction in CoF. At a sliding speed of 10 mm/s, the CoF of the textured sample with four grooves reaches a minimum value of 0.15. Compared with the smooth one, the decreasing amplitude was 7.7%. While for the same total contact length, the more dispersed groove distribution may also lead to the more remarkable friction reduction. Simulation analysis revealed that the primary mechanism for friction reduction was the improved oil supply at the contact line, coupled with a decrease in the shear stress exerted by the fluid domain on the surface. An increase in groove number results in a rise in contact stress, whereas the effect of groove distribution is insignificant.

Keywords

Macro-grooved texture, line contact, reciprocating friction test, coefficient of friction

Date received: 3 March 2025; accepted: 16 July 2025

Introduction

It is estimated that among the total global energy consumption, about 20% is consumed to overcome friction.[1] Reducing friction and wear is the eternal pursuit for human beings. Earlier, the direct method consisted of smoothing contact surfaces, along with the application of lubricants to weaken solid-solid contact. However, recent work has confirmed that the tribopairs with high smoothness is not always the best. On the contrary, the presence of artificial micro-pattens can greatly influence tribological performance of lubricated surfaces.

Actually, as early as 1966, Hamilton et al.[2] first reported that irregular cavities on rubbing surfaces could generate additional load-carrying capacity and thereby reduce the coefficient of friction (CoF). These 'irregular cavities' represent the embryonic form of surface texture. Nowadays, the surface texture, such as micro-dimples or grooves, has been a well-known approach to improve tribological performances of sliding surfaces. Several mechanisms have been proposed to explain the principle of friction reduction. First, the texture can capture the wear debris generated during friction.[3–6] Second, the dimples may store extra lubricating oil[7–9] for secondary lubrication.[10,11] Third, because the texture area has the opportunity to produce cavitation effect,[12,13] which can generate an additional hydrodynamic pressure.

Currently, surface texture has been successfully applied in various mechanical components, such as bearings,[14–16] gears,[17,18] piston rings[19–21] and even human joints.[22–25] Schnell et al.[15] used a femtosecond laser to create V-shaped texture on a bearing surface, with the width of 20 μm and length of 80 μm. Results revealed that the symmetrical texture can significantly reduce friction under both boundary and mixed lubrication conditions. Vladescu et al.[21] conducted reciprocating sliding tests on groove-textured samples with the groove width of 60 μm to simulate the automotive piston ring-liner contact. It was found that the micro-grooves improve

[1]National Key Laboratory of Helicopter Aeromechanics, Nanjing University of Aeronautics and Astronautics, Nanjing, China
[2]College of Mechanical & Electrical Engineering, Nanjing University of Aeronautics & Astronautics, Nanjing, China

Corresponding author:
Wei Huang, College of Mechanical & Electrical Engineering, Nanjing University of Aeronautics & Astronautics, 29# Yudao St., Nanjing 210016, China.
Email: huangwei@nuaa.edu.cn

friction performance over the entire stroke length in thin-film lubrication. Dong et al.[22] fabricated micro-groove with the widths ranging from 55 μm to 190 μm, on CoCrMo femoral heads. The results obtained from pin-on-disc device showed that the CoF of the textured samples got reduced by 20%, when compared with the smooth surface. Braun et al.[26] fabricated pits with diameters ranging from 15 to 800 μm at the surface of C85 steel and employed a pin-on-disc tribo-tester to investigate the effect of texture at different temperatures. The results indicated that the pit diameter of 40 μm was optimal at 100 °C and 200 μm at 50 °C. Yin et al.[27] established CFD model of double-layer composite microtextures and found that wing shape texture had superior friction behavior. Hao et al.[28] analysed a control model of the micro-textured surface and investigated the oil supply mechanism. Zheng et al.[29] studied the mechanisms of surface-textured graphite under water lubrication and found that water molecules trapped in the dimple-type textures can generate additional hydrostatic pressure.

Taking account of the contact configurations, it can be found that the popular studies of surface texturing have focused on the point contact and face-to-face contact, while only a few investigations have been carried out for the line contact. Lu et al.[30] conducted line contact reciprocating experiments on triangular textured samples with a length of side of 250 μm. The results indicated that a peak in the friction force occurs at the boundary of the pits, when the contact region begins to detach. Zhao et al.[18] conducted fluid simulations on textured gears and analyzed the oil film pressure on the tooth surface. The results showed that the CoF of the crescent texture was reduced by over 30%.

Besides the contact configuration, the geometric dimension of the texture is another interesting topic. Recent studies have shown that, not only micron-scale textures, but the textures with the centimeter scale also present the friction-reducing properties. Yin et al.[20] conducted reciprocating friction tests to evaluate the effect of grooves with the width of 2 mm. The results showed that under lubrication conditions, the grooved texture exhibits the lowest average CoF, compared to the pit texture. Wang et al.[31] simulated the rotation bearings using computational fluid dynamics (CFD) method and it was found that the load-bearing capacity decreased by 0.3% and 25.3% corresponding to the width of the squared textures of 1 mm and 2 mm. It was suggested that the significant reduction of contact area may contribute to the friction reduction in face-to-face contact.[16,30,32,33] And how about the micro textures under the line contact condition? There is little knowledge about it.

In this paper, different macro grooves were created on the surface of 45 steel. The reciprocating frictional tests were conducted between cylindrical roller and the grooved surfaces. The actual contact length between the tribopairs was controlled by varying the geometric parameters of the grooves. To analyse the friction reduction mechanism, the contact stress and the distribution of the flow field were also considered. Such an assessment may produce a guideline and better understanding for the application of macro textures to various tribological components.

Methodology

Experimentation

Rectangular samples were machined from 45 steel sheet having length and thickness of 20 mm and 5 mm, respectively. The ultraviolet laser marking machine was used to generate the grooves on the surface of these samples as shown in Figure 1. The applied machine parameters were: power = 4.5 W, current = 1 A, frequency = 40 kHz, and speed = 100 mm/s. The laser pulse generated by fiber laser irradiates on the sample surface and liquid and vapor phases appear in the heated zone. The desired groove textures were formed after the removal of metal and resolidification of the liquid phase. Later, sand paper was used to remove the recast layer and each sample was polished to a surface roughness of Ra 0.2 μm. Finally, the samples were ultrasonically cleaned using absolute ethanol solution. It can be found that the bottom of th groovs is relatively flat and the walls are almost vertical.

Figure 2 presents the geometric parameters and 3D profile of the five types of textured samples, prepared in this study. The depth of each groove was fixed at 40 μm. These samples were divided into two groups: (1) first group was used to explore the actual contact length effect with different groove numbers, and it consisted of samples G1-1, G1-2 and G1-4, having 1, 2 and 4 grooves, respectively. The width and inter-spacing between these grooves were 1 mm. (2) second group was used to figure out the groove distribution effect with the same actual contact length, and it consisted of samples G1-4, G2-2 and G4-l, having the same total groove width of 4 mm. Sample G2-2 consisted of two grooves with the width of 2 mm and groove space of l mm. Sample G4-1 consisted of only one groove with the width of 4 mm. For each of the tests, the smooth sample was used for reference and comparison.

The tribological behavior of macro-textured and smooth surfaces was evaluated using a reciprocating tribometer (Type 32 Surface Property Tester, Shinto Scientific Co., Ltd). And Figure 3 shows the sketch map with a cylinder-on-plate contact configuration (line contact). The GCr15 cylinder with the diameter of 10 mm and length of 8 mm was selected as the upper counter part and it was fixed in a cylindrical holder. The lower grooved specimen was fixed at a reciprocating platform. AeroShell Turbine Oil 555 with the viscosity of 23.3 mPa·s was used as lubricant. Prior to the test, 100 μL of lubricant oil was added to the contact area by using a pipette. Experiments were conducted under a load of 10 N, with the sliding speeds of 1 mm/s, 2 mm/s, 3 mm/s, 5 mm/s and 10 mm/s, respectively. The stroke length was set at 20 mm. Before acquisition of the friction force, an 8-min running-in was conducted to achieve the

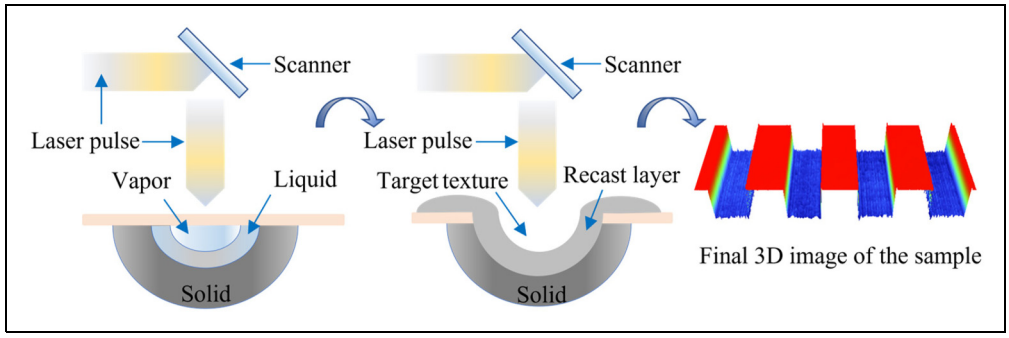

Figure 1. Schematic diagram of material removal by laser processing and final 3D image of the sample.

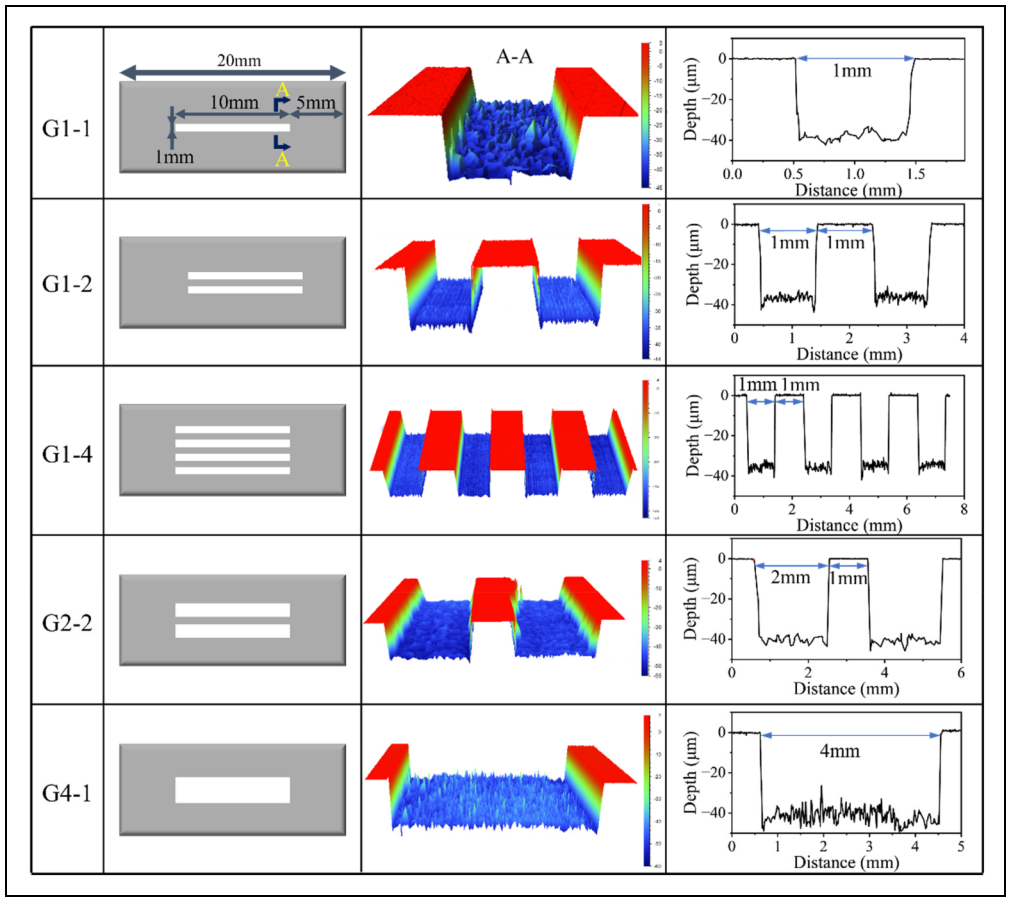

Figure 2. Geometric parameters and three-dimensional morphology of the groove textured samples.

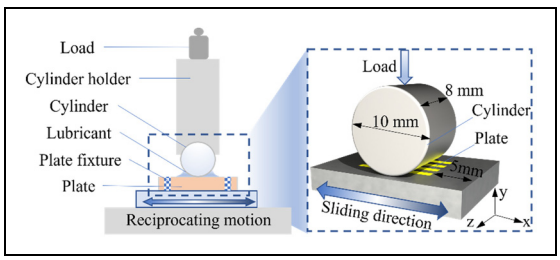

Figure 3. Schematic diagram demonstrating the construction of the reciprocating tribometer and experimental conditions.

stable conditions. Each sample was tested at these five speeds, by increasing the speed after every two minutes. To ensure accuracy, each experiment was repeated three times.

Numerical simulations

To analyze the effect of grooves on contact stress and deformation, a 3D solid model was established using the standard finite element analysis (FEA) software Abaqus, as shown in Figure 4. And it was discretized using a hexahedral mesh, with refinement applied to the contact area. Considering both computational time and accuracy, the core area was set to have a minimum mesh size of 0.017 mm. The boundary conditions are specified as follows: the cylinder had vertical degree of freedom only and was subjected to a concentrated force of 10 N in the downward direction, while the lower sample moved horizontally at 10 mm/s. The CoF was set as a constant value of 0.2 based on the experiment.

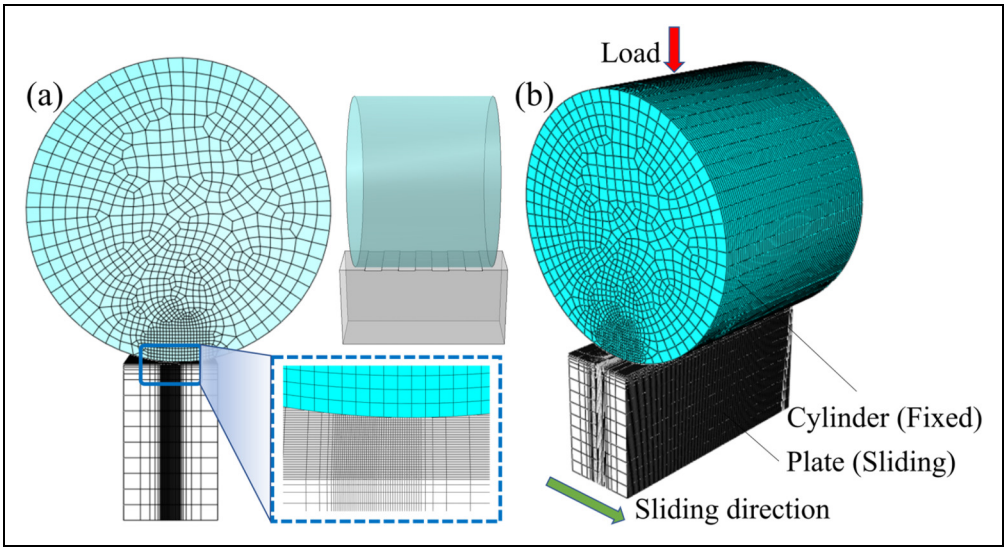

Figure 4. Details of the Abaqus simulation. (a) Abaqus meshing contact model; (b) constraint conditions of the cylinder-on-plate model.

According to Hertz line contact theory, the maximum Hertz contact stress on the contact surface under a 10 N load was calculated to be 94.21 MPa. While the simulation result predicted a contact stress of 96.52 MPa, with an absolute error of 2.4%. Such result confirms the credibility of the simulation.

The influence of macro-texture on lubricant flow was investigated by establishing a finite element model, using Fluent software. Following assumptions were made: (1) The density and dynamic viscosity of the lubricating oil remained constant as 875 kg/m^3 and 23.3 mPa·s, respectively; (2) Gravity was ignored; (3) The contact model was simplified to a smooth surface. The characteristic length of the lubricating oil was 1 mm based on the groove width. The corresponding Reynolds number was determined by equation (1):

$$Re = \frac{\rho u d}{\mu} \tag{1}$$

where Re is the Reynolds number; ρ is the fluid density; u is the fluid velocity; d is the characteristic length and μ is the fluid dynamic viscosity. The calculated Reynolds number was 3.755, which is much lower than 2000.[34,35] Therefore, the fluid flow was considered to be laminar flow.

As shown in Figure 5(a), the length L and width W of the fluid domain were 1 cm and 8 cm, respectively. R is the radius of the cylinder. According to Ref.,[17,36] the oil film thickness h_0 was set as a fixed value of 1 μm. The thickness of the groove (h_1) was 40 μm. Total oil film thickness within the grooved area is the sum of the two values. Figure 5(b) shows the meshed fluid domain. Figure 5(c) presents the mesh sensitivity analysis. With mesh refinement, the maximum and minimum pressures on the upper surface gradually converge. Grid independence verification confirmed that this grid size satisfies the required accuracy. Considering both accuracy and computational efficiency, a mesh count of 218,868 elements was adopted, the minimum grid size was set to 1 μm.

For the fluid domain boundary, following specific boundary conditions were applied[27,34]:

1. The upper surface of the fluid domain is defined as a stationary wall, corresponding to the fixed upper sample. The lower surface is set as a moving wall, sliding in the positive x-direction at a constant speed of 10 mm/s[17] to match the motion of the lower sample.
2. The inlet and outlet boundaries were the inlet and the outlet pressure boundaries, respectively. Based on the actual experimental conditions, the gauge pressure at both boundaries is set to zero.
3. All other walls were considered to be stationary.

According to the law of conservation of mass, the increased fluid mass per unit time is equal to the net mass flowing into the unit at the same time, which can be expressed by equation (2):

$$\frac{\partial \rho}{\partial t} + \nabla \cdot (\rho V) = 0 \tag{2}$$

where ρ is the density of the lubricant, t is the time, and V is the velocity vector.

In this study, the lubricant is considered to be an incompressible fluid with a constant viscosity. The Navier-Stokes (N-S) equation can be expressed as equation (3):

$$\frac{\partial V}{\partial t} + (V \cdot \nabla)V = f - \frac{1}{\rho}\nabla p + \frac{\mu}{\rho}\nabla^2 V \tag{3}$$

where f is the unit volume force vector acting on the lubricant, p is the pressure on the fluid element.

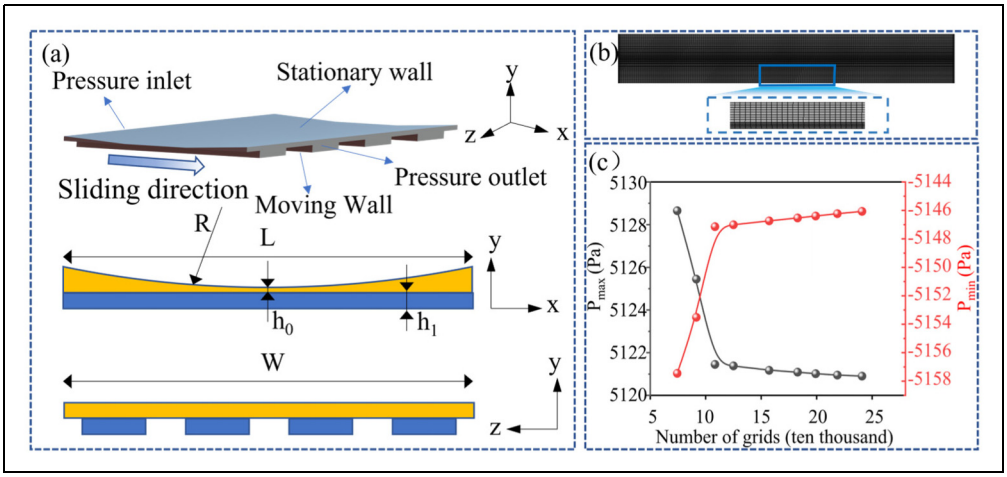

Figure 5. Details of the CFD simulation. (a) schematic diagram of the three-dimensional flow domain model and boundary conditions; (b) mesh independence test results; (c) computational mesh of the fluid domain.

Results and discussion

Tribological behavior of the macro grooved surfaces

Figure 6 presents a comparison of CoF observed for the grooved sample (G1-4) and a smooth surface, over multiple cycles at a speed of 1 mm/s. The sliding distance in a half cycle was 20 mm, which corresponds to the total length of the sample, while the groove (having a length of 10 mm) occppied quarter of the cycle. CoF was observed to remain stable at a value of about 0.2 for the smooth sample, in each cycle. While for the textured sample, the CoF exhibited a value of 0.2 at the beginning of the cycle as the cylinder slides over the smooth surface. While it reduced to 0.17 when the cylinder sliding over the groove. This behavior is consistent with the Zimmer's experimental results,[32] which presented that the grooves may act to increase oil entrainment into the rubbing surface, and hence reduces asperity contact. After that, the CoF again increased to a value of 0.2 as it sliding out of the grooved area. And the increment in CoF can be attributed to the lubricant film being steadily squeezed out of the contact area. This phenomenon repeats periodically within multiple cycles motion. Such results preliminarily demonstrate that the macroscale texture does present the friction reduction effect.

To gain a further insight into this phenomenon and to explore the effect of total groove width spaned by the contact line on the CoF, tribological tests were carried out using the following four samples: a smooth sample, G1-1, G1-2, and G1-4.

Figure 7 shows the variations in CoF for the four samples, sliding in a half-cycle at different speeds. Generally, as the cylinder entered the grooved area, a reduction in CoF was observed for all of the tested conditions. The contact line length of the friction pair for the smooth sample equals to the length of the cylinder, which is 8 mm. The contact line lengths of the three grooved samples, G1-1, G1-2, and G1-4, are 7 mm, 6 mm, and 4 mm, respectively. CoF was observed to

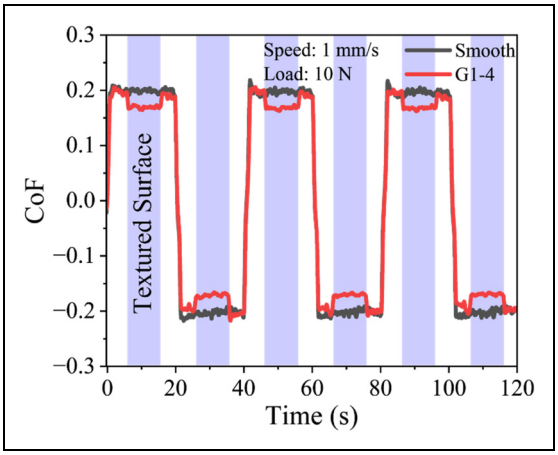

Figure 6. Comparison of CoF observed in smooth sample and textured sample (G1-4), over multiple cycles.

decrease with a decrease in actual contact line of the tribopair.[30] According to the value of the CoF, the friction may run at boundary and mixed lubrication regimes. Due to the insufficient lubricant entrainment, the CoF may be dominated by the asperity contact. With the increase in the groove number, the actual contact line between the tribopairs decreases. As a result, the shorter of the contact line, the less contact of the asperity. In addition, the decrease of the contact line may also lead to the increase of the stress and deformation. Therefore, more lubricant may flow into the contact area due to the squeeze film effect.[21] Secondary lubrication acts under mixed lubrication conditions.[19] The oil reserved in the grooves is a secondary source of lubricant, helping to reduce frictional resistance. Thus, the sample (G1-4) presented the lowest average CoF during the half-cycle, while the smooth sample exhibited a relatively stable CoF throughout the half-cycle.

To investigate the effect of groove distribution with the same contact line length on the CoF, samples G1-4, G2-2,

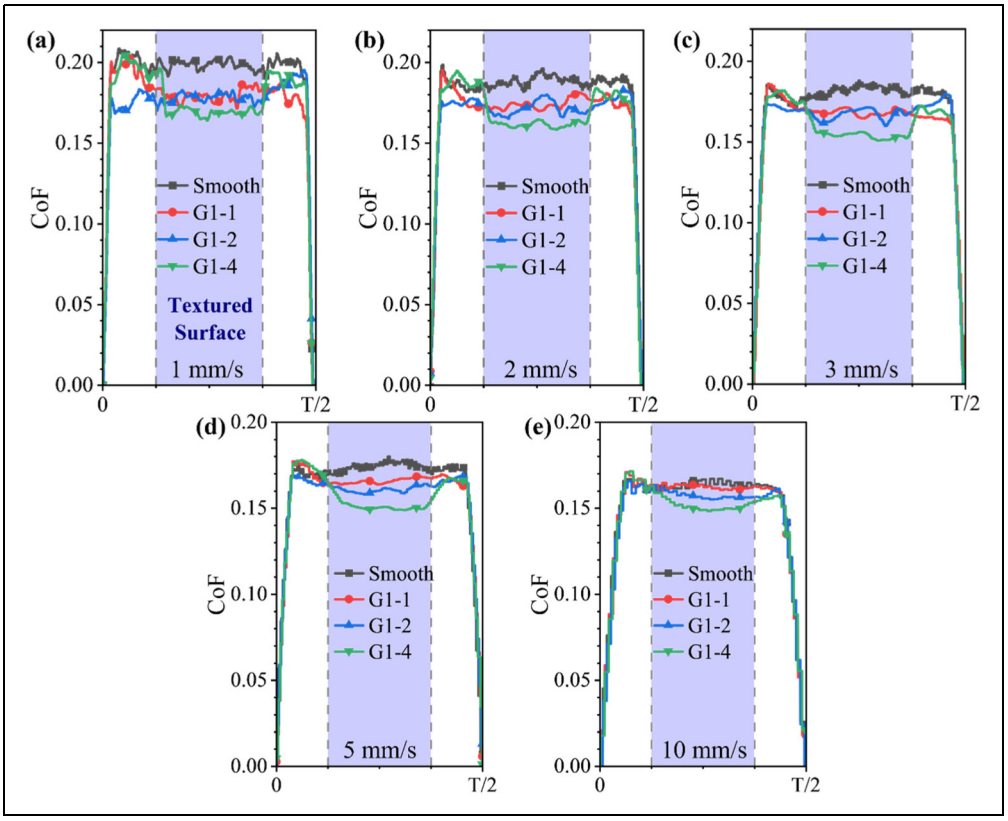

Figure 7. Cof in the half-cycle for different contact line lengths at various sliding speeds.

and G4-1 were applied with the same total groove width (4 mm). Figure 8 shows the CoF over half cycle under different speed conditions. The three groove distributions demonstrated positive friction reduction benefits, ranked as G1-4, G2-2, and G4-1 based on the magnitude of friction reduction.

As shown in Figure 8, compared to the smooth surface, all three macro-textures caused a reduction in the CoF. The three types of groove distribution exhibited varying friction reduction capabilities under each speed condition. For the same sample, the CoF decreases as the speed increases. Hence, the distribution of macro-textures significantly influences the CoF. For the same contact line length, as the groove becomes more dispersed, the CoF decreases accordingly.

Figure 9 illustrates the summary of the CoF for varying contact line lengths and distributions at different sliding speeds. In general, the CoF reduces with a decreasing of actual contact line length and it decreases as the groove distribution becomes more dispersed. In addition, the trend in the CoF variation aligns with the mixed lubrication section of the Stribeck curve, where the CoF decreases with the increasing speed. Hence it was concluded that macro-textures may reduce the CoF in line contact under low-speed conditions.

Contact stress and deformation in line contact

To investigate the effect of grooves on the contact stress and deformation, a simulation model was established. Figure 10 presents the contact stress and deformation along the contact line direction. It is known that the existence of textures can notably increase the contact stress between friction pair.[18] As expected, stress concentrations occur on both sides of the grooves, as shown in Figure 10(a) and (b). Meanwhile, the corresponding deformations also increased as presented in Figure 10(c) and (d). The areas of stress concentration aligns with the location of maximum local deformation. The friction reduction is likely due to the combined effects of deformation and friction as the cylinder sliding over the groove area. The local deformation may facilitate lubricant flow from the groove to the contact area. In the groove region where the cylinder slides, the recovery of local deformation helps retain the lubricant on the surface, as pointed in Ref.[9] Thus, the more lubricant may maintain on the sliding surface to decrease the friction due to the squeezing effect.

As shown in Figure 10(a), with the increase of the groove numbers, locations and values of the stress concentration increase. Therefore, the oil supply points in the contact region also enhance. In addition, the higher of the deformation (Figure 10(c)), the larger of the oil mass supply. In this case, more lubricant overflows in the contact area and the lubrication mechanism of the groove is more likely to exhibit a secondary lubrication effect.[19,37] Thus, the decrease of the actual contact line length lead to the reduction of CoF.

Figure 10(b) and (d) present the stress and deformation results for different groove distributions with the same

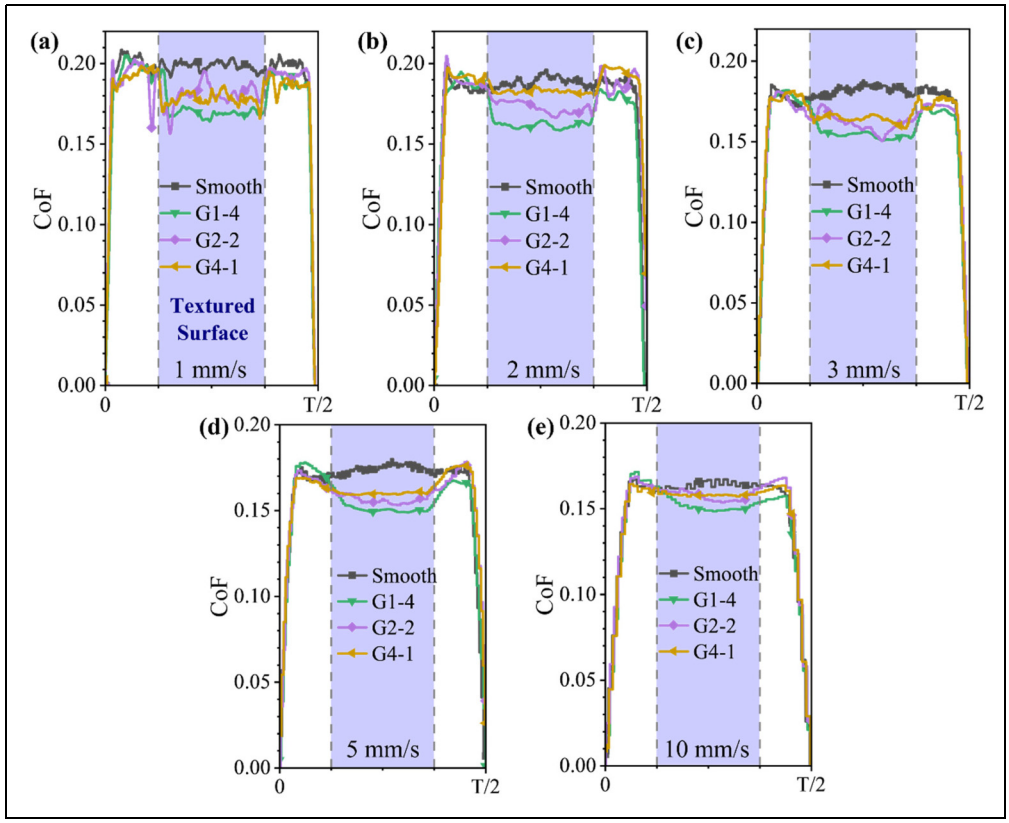

Figure 8. Cof in the half-cycle for different groove distributions at various sliding speeds.

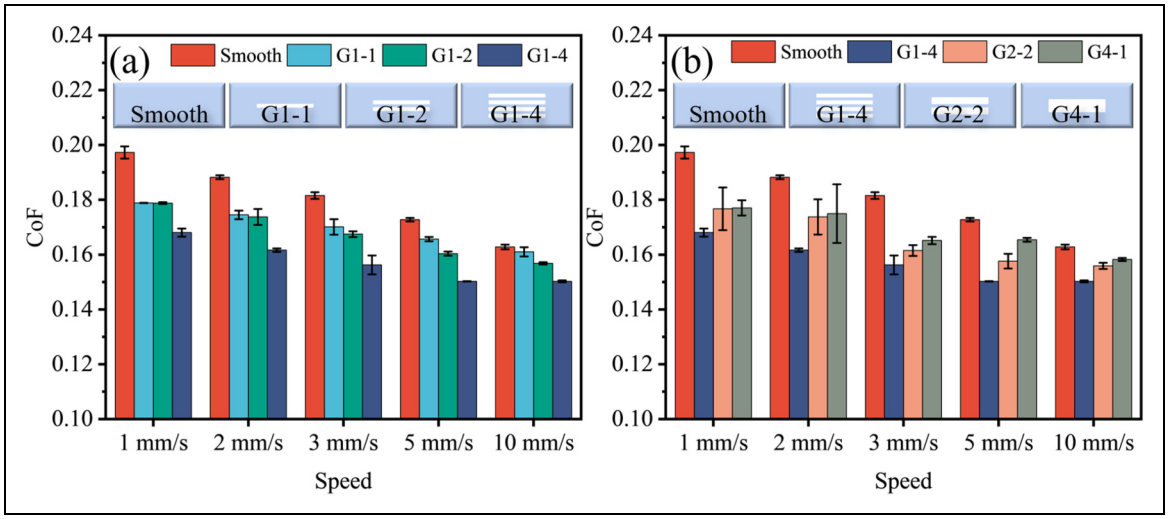

Figure 9. Summary of CoF for (a) varying contact line lengths and (b) varying groove distributions at different sliding speeds.

contact line length. It seems that with the decrease of groove number, local contact stress and deformation increase. Sample G1-4 exhibits the lowest stress and deoformation with more even distribution. Compared with the result in Figure 10(c), the deformation of the three types of groove distribution is relative close. Based on the the experimental results, it can be deduced that compared with the deformation, the oil supply points along the contact line may play as the dominated effect. Therefore, sample G1-4 expresses the best tribological behavior.

Flow field in line contact

To figure out the effect of grooves on the flow of lubrication, the fluid simulation was carried out. According to the geometric model (shown in Figure 5), the oil film thickness in the textured region of the fluid domain increased

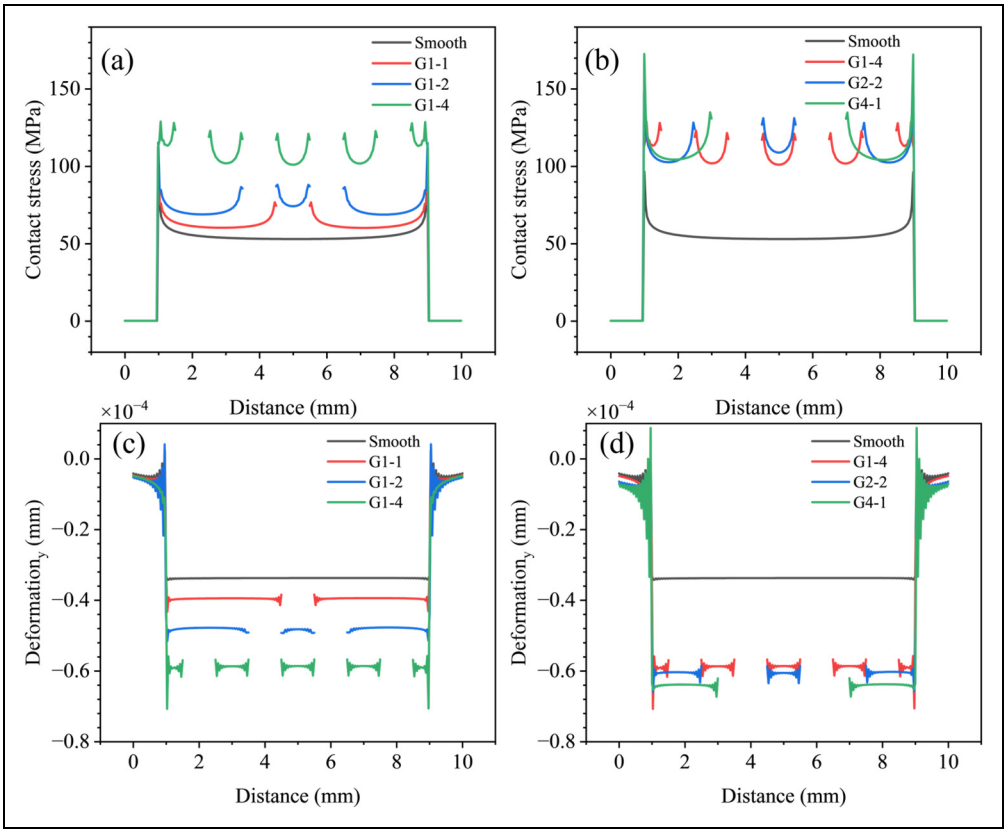

Figure 10. Effect of grooves on stress and deformation. (a) contact stress with varying contact line lengths; (b) contact stress with different grooves distribution; (c) deformation with varying contact line lengths; (d) deformation with different grooves distribution.

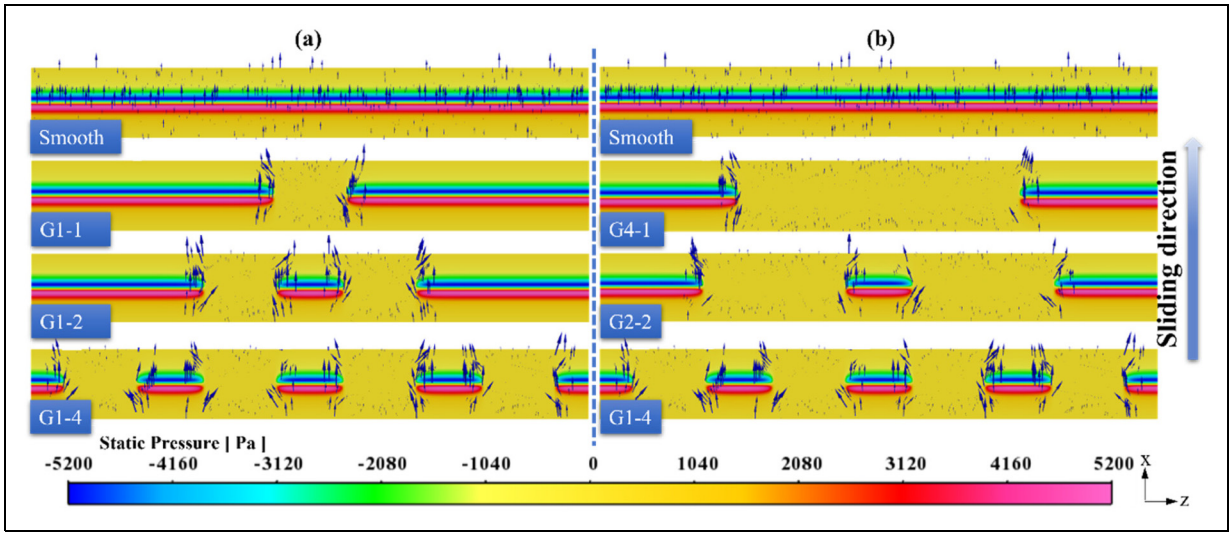

Figure 11. The pressure distribution and local velocity vector diagrams for varying contact line lengths and distributions. (a) sample with varying contact line lengths; (b) sample with different groove distributions.

from h_0 to $h_0 + h_1$. As pointed in Ref.,[38] shear stress (τ) can be defined as $\tau \approx \eta V / (h_0 + h_1)$. The reduction in τ took place within the grooved region, leading to a reduction in the CoF. Consequently, the velocity and pressure gradients along the oil film thickness direction in the grooved region were minimal. This implies that the area available for lubricant shear got reduced, resulting in decreased contact frictional force.[32]

Figure 11 presents the horizontal section of the fluid domain. The pressure in the groove area lies between the high and low pressure regions. These pressure variations were primarily caused by the oil first entering the convergent wedge region. The oil film thickness reduced, while the pressure increased rapidly, thus creating the high-pressure region. Later, the oil flows into the divergent wedge region, where the oil film thickened

and the pressure decreased. The oil flows from the high-pressure region to the low-pressure region. As shown in Figure 11, lubricating oil followed arcuate paths on both sides of the groove. Over the slided area, the oil on both sides of the groove first flowed inward, while ahead the contact aera, the oil inside the groove flowed outward. Therefore, the grooved texture helped to supply additional oil to the contact line.

As shown in Figure 11(a), with the decreasing of the actual contact length, more locations for oil supply were created, leading to a decrease in the CoF. Besides, based on the simulation result, for each grooved sample, the flow velocity of the lubricant in z-axis direction is independent of the groove numbers. It means that increasing of the groove number may also improve the ability of oil supply. Figure 11(b) shows the simulation results with different groove distributions. The lubricating oil followed arcuate paths on both sides of the groove. Despite the same contact length, the different groove distribution increased the number of oil supply positions from 2 to 8, enhancing the oil supply and thus reducing the CoF.

Conclusions

This study combined experimental and numerical simulation methods to investigate the impact of macro-textures on the CoF in line contact, and to examine the variations in the actual contact line and their influence on friction. Based on the findings, the following conclusions can be drawn:

1. An increase in the number of groove textures results into a decrease in CoF. In addition, the CoF of all grooved samples shows a general decreasing trend with increasing sliding speed. In particular, the sample with four grooves (G1-4) exhibits the lowest CoF of 0.15 at a sliding speed of 10 mm/s, which is 7.7% lower than that of the smooth one. At low speed of 1 mm/s, G1-4 still shows the highest friction reduction of 14.8%, compared with smooth surface.
2. For the same contact line length, the more dispersed distribution of grooves presents the better tribological performance. Among three textured samples G1-4, G2-2, and G4-4, the sample with four grooves (G1-4) exhibited the lowest CoF. Similarly, the CoF of all the samples decreases as the sliding speed increases.
3. The numerical simulation also predicted that under line contact conditions, the primary mechanism for friction reduction is the supply of lubricant in the deformed contact area and the arcuate flow induced by the pressure gradient. Ideally, macro-textures should be more widely distributed with multiple grooves to achieve a lower CoF.

Acknowledgements

The authors thank the National Key Laboratory of Helicopter Aeromechanics Funding (2024-CXPT-GF-JJ-093-03) and National Natural Science Foundation of China (No. 52175172) for financial support.

Declaration of conflicting interests

The authors declared no potential conflicts of interest with respect to the research, authorship, and/or publication of this article.

Funding

The authors disclosed receipt of the following financial support for the research, authorship, and/or publication of this article: This work was supported by the National Natural Science Foundation of China, National Key Laboratory of Helicopter Aeromechanics Funding, (grant number No. 52175172, 2024-CXPT-GF-JJ-093-03).

ORCID iDs

Wei Huang https://orcid.org/0000-0002-8871-634X
Xiaolei Wang https://orcid.org/0000-0002-9055-1011

References

1. Holmberg K and Erdemir A. Influence of tribology on global energy consumption, costs and emissions. *Friction* 2017; 5: 263–284.
2. Hamilton DB, Walowit JA and Allen CM. A theory of lubrication by microirregularities. *J Basic Eng* 1966; 88: 177–185.
3. Xing Y, Deng J, Feng X, et al. Effect of laser surface texturing on Si3N4/TiC ceramic sliding against steel under dry friction. *Mater Des* 2013; 52: 234–245.
4. Shimizu J, Nakayama T, Watanabe K, et al. Friction characteristics of mechanically microtextured metal surface in dry sliding. *Tribol Int* 2020; 149: 105634. doi:10.1016/j.triboint.2019.02.042
5. Kumar M, Ranjan V and Tyagi R. Effect of shape, density, and an array of dimples on the friction and wear performance of laser textured bearing steel under dry sliding. *J Mater Eng Perform* 2020; 29: 2827–2838.
6. Zhu Y, Chen J, Du J, et al. Tribological behavior of laser textured nodular cast iron surface. *Ind Lubr Tribol* 2019; 71: 949–955.
7. Tang Z, Liu X and Liu K. Effect of surface texture on the frictional properties of grease lubricated spherical plain bearings under reciprocating swing conditions. *Proc IMechE Part J: J Engineering Tribology* 2016; 231: 125–135.
8. Ma J, Liu Y, Mostaghimi J, et al. Effect of laser-induced texture on lubrication retention and tribological properties of 40Cr alloy surfaces. *Tribol Int* 2023; 187: 108651. doi:10.1016/j.triboint.2023.108651
9. Wang W, Zhao W, Guo P, et al. A textured surface with oil inflow and outflow function designed for starved lubrication. *Tribol Int* 2023; 184: 108450. doi:10.1016/j.triboint.2023.108450
10. Li C, Yang X, Wang S, et al. Study on friction and lubrication characteristics of surface with unidirectional convergence texture. *Coatings* 2019; 9: 780. doi:10.3390/coatings9120780
11. Liu Y, Zhang H, Dai S, et al. Designing a bioinspired scaly textured surface for improving the tribological behaviors of starved lubrication. *Tribol Int* 2022; 173: 107594. doi:10.1016/j.triboint.2022.107594
12. Jamari J, Muchammad M, Hilmy F, et al. Effect of inertia on the cavitation phenomena of hydrodynamic textured

bearings considering slip. *J Braz Soc Mech Sci Eng* 2019; 41: 387. doi:10.1007/s40430-019-1890-9
13. Sun H, Yan Z, Wu S, et al. A study on the cavitation effect of elastic material with textured surfaces under fluid lubrication conditions. *Machines* 2024; 12: 267. doi:10.3390/machines12040267
14. Wang Y, Jacobs G, Zhang S, et al. Lubrication mechanism analysis of textures in journal bearings using CFD simulations. *Ind Lubr Tribol* 2024; 77: 2–14. doi:10.1108/ilt-01-2024-0031
15. Schnell G, Studemund H, Thomas R, et al. Experimental investigations on the friction behavior of partially femtosecond laser-textured journal bearing shells. *Tribol Int* 2023; 188: 108764. doi:10.1016/j.triboint.2023.108764
16. Profito FJ, Vladescu SC, Reddyhoff T, et al. Numerical and experimental investigation of textured journal bearings for friction reduction. *Tribol Int* 2024; 195: 109643. doi:10.1016/j.triboint.2024.109643
17. Chang X, Renqing D, Liao L, et al. Study on hydrodynamic lubrication and friction reduction performance of spur gear with groove texture. *Tribol Int* 2023; 177: 107978.
18. Zhao T, Wang Y, He Y, et al. Numerical simulation and experimental investigation on tribological properties of gear alloy surface biomimetic texture. *Tribol Trans* 2023; 66: 610–622.
19. Grabon W, Koszela W, Pawlus P, et al. Improving tribological behaviour of piston ring–cylinder liner frictional pair by liner surface texturing. *Tribol Int* 2013; 61: 102–108.
20. Yin H, Zhang X, Guo Z, et al. Synergetic effects of surface textures with modified copper nanoparticles lubricant additives on the tribological properties of cylinder liner-piston ring. *Tribol Int* 2023; 178: 108085. doi:10.1016/j.triboint.2022.108085
21. Vladescu S-C, Olver AV, Pegg IG, et al. The effects of surface texture in reciprocating contacts – an experimental study. *Tribol Int* 2015; 82: 28–42.
22. Dong Y, Svoboda P, Vrbka M, et al. Towards near-permanent CoCrMo prosthesis surface by combining micro-texturing and low temperature plasma carburising. *J Mech Behav Biomed Mater* 2016; 55: 215–227.
23. Tewelde FB, Allen Q and Zhou T. Multiscale texture features to enhance lubricant film thickness for prosthetic hip implant bearing surfaces. *Lubricants* 2024; 12: 187. doi:10.3390/lubricants12060187
24. Kumar V, Tewari RP and Rawat A. Machine learning-based investigations of the effect of surface texture geometry on the wear behaviour of UHMWPE bearings in hip joint implants. *Biosurf Biotribol* 2024; 10: 143–158. 10.1049/bsb2.12085
25. Modica F, Basile V, Surace R, et al. Replication study of molded micro-textured samples made of ultra-high molecular weight polyethylene for medical applications. *Micromachines (Basel)* 2023; 14: 523. 10.3390/mi14030523
26. Braun D, Greiner C, Schneider J, et al. Efficiency of laser surface texturing in the reduction of friction under mixed lubrication. *Tribol Int* 2014; 77: 142–147.
27. Yin H, Yang J and Gu Q. Numerical study on the hydrodynamic lubrication performance improvement of bio-inspired peregrine falcon wing-shaped microtexture. *Tribol Int* 2024; 191: 109049. 10.1016/j.triboint.2023.109049
28. Hao M, Fan Y, Li B, et al. Influence of oil supply on the friction state of the micro-textured surface of the sliding guide. *Ind Lubr Tribol* 2025. 10.1108/ilt-12-2024-0459
29. Zheng C, Yang Y, Cheng S, et al. Friction reduction and anti-wear mechanisms of surface-textured graphite under water lubrication. *Wear* 2025; 562-563: 205665. 10.1016/j.wear.2024.205665
30. Lu P, Wood RJK, Gee MG, et al. A novel surface texture shape for directional friction control. *Tribol Lett* 2018; 66: 51. 10.1007/s11249-018-0995-0
31. Wang Y, Jacobs G, König F, et al. Investigation of microflow effects in textures on hydrodynamic performance of journal bearings using CFD simulations. *Lubricants* 2023; 11: 20. 10.3390/lubricants11010020
32. Zimmer M, Vlădescu S-C, Mattsson L, et al. Shear-area variation: A mechanism that reduces hydrodynamic friction in macro-textured piston ring liner contacts. *Tribol Int* 2021; 161: 107067. 10.1016/j.triboint.2021.107067
33. Urabe M, Takakura T, Metoki S, et al. Mechanism of and fuel efficiency improvement by dimple texturing on liner surface for reduction of friction between piston rings and cylinder bore. Report no. 0148-7191, 2014. SAE Technical Paper. DOI: 10.4271/2014-01-1661.
34. Li Y, Zhang Z, He Y, et al. Research on internal flow field characteristics of straight-groove texture using three-dimensional modeling. *Lubricants* 2023; 11: 338. 10.3390/lubricants11080338
35. Wang Z, Chen W, Zhang L, et al. Surface texture and heat treatment on the friction performance of cam tappet experimental and fluid-solid coupling numerical study. *Tribol Int* 2023; 179: 108124. 10.1016/j.triboint.2022.108124
36. Duoji R, Shanming L and Xuefeng C. Study on hydrodynamic lubrication and friction reduction performance of cylindrical rolls with tesla valve texture. *Tribol Trans* 2023; 66: 1–11. DOI: 10.1080/10402004.2023.2249955
37. Wang XL, Kato K, Adachi K, et al. Loads carrying capacity map for the surface texture design of SiC thrust bearing sliding in water. *Tribol Int* 2003; 36: 189–197. Article.
38. Scaraggi M, Mezzapesa FP, Carbone G, et al. Minimize friction of lubricated laser-microtextured-surfaces by tuning microholes depth. *Tribol Int* 2014; 75: 123–127.